Iranian Journal of Electrical and Electronic Engineering

Journal Homepage: ijeee.iust.ac.ir

Research Paper

Eccentricity Fault Modeling and Diagnosing of PMSM Using the Magnetic Equivalent Circuit Model

V. Naeini* (C.A.), and M. Moomeni*

Abstract: This paper introduces the modeling and fault diagnosis of rotor eccentricities of permanent magnetic synchronous machine (PMSM). The modeling of machine in healthy and fault condition have been proposed based on magnetic equivalent circuit (MEC). Nevertheless, the research methods of diagnosis and modeling are common, this paper tends to provide a fast computation and more detailed model with reasonable degree of accuracy. Firstly, the MEC modeling of PMSM in the electric and magnetic fields are introduced and next, the different fault conditions are carried out. Also to consider the eccentricity fault of an interior mounted PMSM, a methodology based on MEC is proposed. The accuracy of this model will be verified by comparing with identical results obtained by finite element method (FEM).

Keywords: Magnetic equivalent circuit (MEC), Permanent Magnetic Synchronous Machine (PMSM), magnetic saturation, eccentricity, finite element method (FEM).

1 Introduction

CHOOSING an accurate and trusted modeling for evaluating the performance of electrical machines with healthy and fault conditions, is very necessary for any study. Varied techniques have been proposed in literature to investigate the electromagnetic performance of electrical machines. Mostly the popular electrical machine modeling techniques are classified in two general parts and typically use the analytical and numerical methods to solve the electromagnetic equations [1]-[11]. Herein, analytical methods are sensorial, quick and nearly non-accurate to evaluate the performance of electrical machines [1]-[5], versus the numerical methods are actual, more accurate and needful computation time [6]-[14].

Iranian Journal of Electrical and Electronic Engineering, 2023. Paper first received 19 Jun 2022, revised 28 Aug 2022, and accepted 13 Sep 2022.

*The authors are with Department of Electrical Engineering, Malayer University, Malayer, Iran.

E-mails: vnaeini@malayeru.ac.ir and m.moomeni@gmail.com.

Corresponding Author: V. Naeini.

https://doi.org/10.22068/IJEEE.19.1.2568

Ignoring the geometry, curvature and tangential component of magnetic flux in analytical methods, especially when the air-gap length is not sufficiently small, result to considerable wrongs [2]. In other words, in cases where accuracy is a major intention, analytical techniques are not suggested. Accordingly, when the details of electrical machine performance are essential, the numerical models are preferred. The main advantages of numerical method are considering the real features as nonlinear magnetization curve of core, complex geometries, flux fringing effect and skewed slots, but are computationally demanding. But, due to the long computing time required of the numerical methods, these techniques are not well suited where intensive computational effort is necessary as the online controlling of machine output, machine optimization process and so on.

The recent researches indicate that, the most encouraging numerical methods are winding function theory (WFT) [12-13], conformal mapping (CM) [14], magnetic equivalent circuit method (MEC) [6]-[11] and finite element analysis (FEA) [12]-[14]. However, the WFT and CM techniques,

are non-precise methods as not able to model the core saturation effect and the air gap of electrical machine which are practically the main defects of the WFT and CM for detailed model such as eccentricity fault. Conversely the finite element method (FEM) can exactly model the electrical machines performance in different conditions. However, due to the FEM method is computationally intensive time-consuming, this technique commonly is used to verify the analytical model in conclusive study step. Moreover, the MEC modeling features such as the capability of machine geometry modeling and containing the time harmonics, which caused this technique to be accurate, fast and moderate complexity to evaluate the performance of electrical machines [7].

Accordingly, the MEC modeling is a preferred technique in variety healthy and faulty conditions such as skewed slots, deep bar contracture, core saturation and hysteresis, short circuit and open circuit faults, end winding leakage flux, torque and voltage ripples in a different machine [15-16]. Furthermore, there are lots of considerable works on MEC modeling of resolvers, in recent years [17–18].

On the other hand, the mechanical faults generally included the air gap eccentricity, are common faults of the electrical machines, which contribute to almost 40–50% of all machine faults [19], and can be occurred due to environmental vibrations, rotor misalignment, overload and so on. Therefore, it is particularly significant to study this fault modeling and detection of PMSM. So far, different techniques have been used to modeling the rotor eccentricity fault in the electrical machines [20]-[27]. Hence, by attention to the advantages of the MEC modeling in variety healthy and faulty conditions, to propound eccentricity fault of an interior PMSM, a methodology based on MEC is proposed in this paper. The presented model according to the previous works is a detailed model where considering the static and dynamic rotor eccentricities. In this modeling, the variable geometrical parameters and the nonlinear phenomenal such as core saturation, slot structure, space harmonics, are considered. Therefore, the provided model is an accurate and fast solution for analysis of machine in the rotor eccentricity diagnostic process.

The purpose of this paper is first, to explain the MEC modeling of machine in healthy and rotor eccentricity conditions and then, to illustrate the variations frequency between the influences of static and dynamic rotor eccentricities on the unbalanced magnetic force (UMF). It will be shown that the MEC model results are closer to the FEM model results and can be a proper substitution to the FEM in machine modeling under fault and fault diagnosis process.

2 Interior PMSM Modeling

2.1 Magnetic equivalent circuit technique

In this section the reluctance network of an interior PMSM is provided by choosing the suitable elements and parameters in numerical method of MEC technique. Moreover, the accuracy of the presented MEC modeling depends on the number of flux tubes and their relationship in the reluctance network. As well as, expected results accuracy of the proposed modeling depends on the mathematical formulation based on the flux tubes behaviors.

After defining all probable flux paths in machine construction, suitable reluctances or permeances are determined for each flux tubes, according to their material, dimensions and nonlinear behavior. Hence, the presented relations for flux tubes of magnetic core sections that have a magnetic saturation phenomenon are inherently nonlinear and in the air gap distance where are function of the rotor position, are parametrically nonlinear. The other types of permeances that have constant geometry and linear permeability, are constant permeances.

Consequently, a reluctance network is created with a set of nodes and loops in which the KVL and KCL equations can be determined using circuit theorems. This method has been performed in different references for various electric machines in similar ways. Fig. 1 shows the schematic of the interior mounted PMSM studied in this paper.

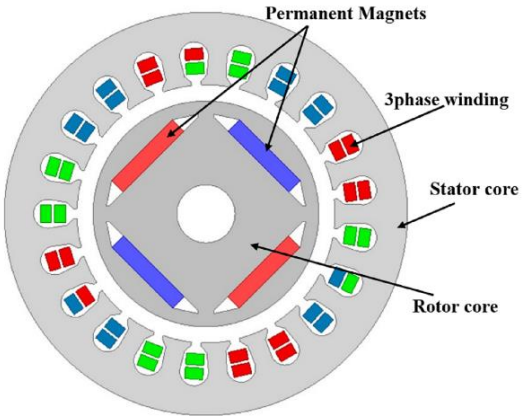

Fig. 1 General schematic of interior mounted PMSM.

According to the above description, a part of the magnetic equivalent circuit of this machine is developed as shown in Fig. 2. As can be seen in this figure, the nonlinear reluctances are used for all iron parts and the linear magnetic permeances are used for the air gap between the stator teeth. Also, the nonlinear parametric permeances depending on the position of the rotor are used between the stator and rotor cores. In terms of circuit theory, a permanent material acts as a constant flux sources that, can be represented by a mmf source in series with constant reluctance.

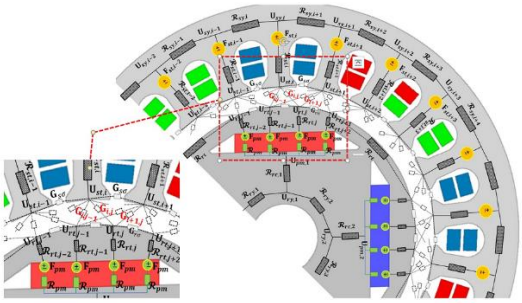

Fig. 2 A part of the magnetic equivalent circuit of PMSM.

According to the above explanations about the equivalent circuit, two points are very important. First, providing a suitable and accurate mathematical relation for nonlinear reluctances of core to be able to model the core saturation behavior, appropriately. Secondly, the relationships of the air gap permeances have a periodic manner as the rotor is rotating. For this purpose, the selection of these elements is done as follows.

For obtaining the air gap permeances relations between the rotor and the stator cores, first the behavior of these permeances, for example between the i-th-stator tooth and the j-th rotor tooth, $G_{i.j}$, are evaluated as shown in Fig. 3.

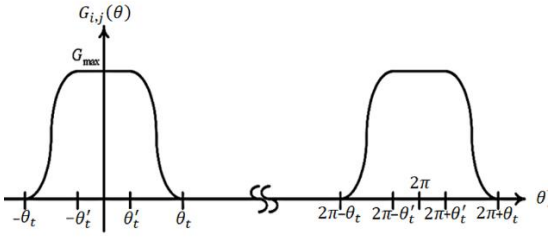

Fig. 3 The air gap permeances approximation, $G_{i.j}$.

As can be seen in this diagram, when both the stator tooth and the rotor tooth completely overlap with each other, the magnetic conduction is formed completely, and by passing these teeth in front of each other, this overlap condition and magnetic conductivity decreases. This behavior is repeated with each rotation of the rotor and thus the air gap permeances relationships must be periodic. Consequently, the relation of $G_{i.j}$, is performed as:

$$G_{i,j}(\theta)=\begin{cases} G_{max} & 0<\theta<\theta'_t \ . \ 2\pi-\theta'_t<\theta<2\pi \\ G_{max}\dfrac{U[-0.81+\cos(\theta)]\times(1+\cos(10\theta))}{2} & \theta'_t<\theta<\theta_t \ . \ 2\pi-\theta_t<\theta<2\pi-\theta'_t \end{cases} \quad (1)$$

where, U[θ] is the unit step function, θ is the rotor position and G_{max} is the maximum air gap permeance where the stator and rotor poles are alignment. The periodic property of Cosine function in $G_{i.j}$, cause to have a periodic manner.

Also the constant permeances relations between the stator teeth which, have constant topology and permeability, are obtained as:

$$G_{s\sigma}=\frac{l_{sa}}{A_{sa}*\mu_0} \quad (2)$$

Moreover, the various relation can be used for the nonlinear behavior modeling of the core magnetic saturation, but the convenient way that proposed previously [9-10], is the reluctance relation of the core flux tube as:

$$\Re(B)=\frac{L}{\mu(B)A}=\frac{10^{-3}\ L}{A\ \mu_0\ e^{-0.8\times B^2}} \quad (3)$$

where L and A are the length and the cross section of the different parts of the stator and the rotor cores, and B is the flux density of the core different parts and $\mu(B)$ is the core permeability that was done in various form in different literatures that in this paper, the above relation is used. The reluctances of the permanent magnet part of the rotor poles are also modeled according to the fixed geometry and the permeability coefficient close to one as following relation:

$$\Re_{pm}=\frac{L_{pm}}{\mu_0 A_{pm}} \quad (4)$$

where L_{pm} and A_{pm} are the length and the cross section of the different parts of the PM poles.

Another important point is to determine the sources of magnetic potential, namely MMF, in an exact equivalent reluctance network. So, the correct

choice of these sources is very essential to attain the correct answer. In the equivalent circuit of a PMSM machine, there are two categories of magnetic potential sources. One of them is the magnetic source on the stator side, which determines the relationship of three-phase currents in the magnetic equivalent circuit, namely ($\mathcal{F}_{\mathrm{si}}$). According to Ampere Law and choosing a contour between two adjacent teeth, each of these sources is determined equal to the algebraic sum of ampere turn flowing inside the same contour. For this reason, determining the winding map in this section is very important. Another category of magnetic sources is the MMF sources of the permanent magnet poles, namely ($\mathcal{F}_{pm}$) which have constant relations, according to their magnetic properties.

In this way, the reluctance network of machine is obtained by specifying the elements of the magnetic equivalent circuit and considering the possible paths of fluxes. According to the circuit analysis theory and evaluating the KVL and KCL equations for every mesh and node of presented reluctance network, unknown variables such as fluxes, could be solved. One category of these equations is in the form of algebraic relations pertaining to the loops and nodes in the equivalent circuit and the other category is the differential equations between the fluxes passing through the phase coils and their induced voltages. These equations are derived as flowing:

2.1.1 The Magnetic Algebraic Equations of PMSM

As mention above, the magnetic algebraic equations are included the loops and nodes equations and due to the high number of air gap permeances, cause a lot of loops equations. Thus, the node magnetic potential equations (KCL) to each air gap nodes of the stator and rotor cores are applied. Hence, by attention to Fig. 2, the KCL's law of magnetic fluxes in i-th stator and in j-th rotor air gap nodes can be obtained respectively as:

$$\varphi_{st.i} = 2u_{st.i}G_{s\sigma} - u_{st.i+1}G_{s\sigma} - u_{st.i-1}G_{s\sigma} + u_{st.i}\sum_{j=1}^{16} G_{i.j} - \sum_{j=1}^{16} u_{rt.j}G_{i.j} \quad (5)$$

$$\varphi_{rt.j} = 2u_{rt.j}G_{r\sigma} + u_{rt.j+1}G_{r\sigma} + u_{rt.j-1}G_{r\sigma} + u_{rt.j}\sum_{i=1}^{21} G_{i.j} - \sum_{i=1}^{21} u_{st.i}G_{i.j} \quad (6)$$

where $\varphi_{st.i}$, $\varphi_{rt.j}$, $u_{\mathrm{st}.i}$ and $u_{\mathrm{rt}.j}$ are the i-th stator tooth flux, the j-th rotor section flux, i-th magnetic potential of stator tooth and j-th magnetic potential of rotor section in the air gap respectively. Also, $G_{s\sigma}$ and $G_{r\sigma}$ are the constant permeances of stator and rotor cores in in the air gap respectively.

Furthermore, due to the Fig. 2, the number of circuit loops in the stator and rotor cores is low and thus, the mesh magnetic potential equations (KVL) to each loops of the stator and rotor cores are applied. The KVL's law of magnetic fluxes in i-th stator loops of the stator yoke and in j-th rotor loops of rotor section above PM poles can be obtained respectively as Eqs. (7) and (8).

where $\varphi_{sy.i}$ and $\mathcal{F}_{\mathrm{st}.i}$ are the i-th stator yoke flux and the i-th MMF of stator tooth respectively, and $\varphi_{pm.j}$ and R_{pm} are the j-th PM flux and the reluctance of PM poles respectively. Also, R_{st} , R_{sy} , R_{rt} and R_{ry} are the inherently nonlinear reluctances of stator and rotor cores respectively and as seen, these reluctances are dependent on core fluxes. The general form of the KVL equations in the adjacent PM poles parts of the rotor can be written as Eq. (9):

$$\mathcal{F}_{st.i} - \mathcal{F}_{st.i-1} = R_{sy.i}\left[\frac{\varphi_{sy.i}}{A_{sy}}\right] * \varphi_{sy.i} + R_{st.i}\left[\frac{\varphi_{st.i}}{A_{st}}\right] * \varphi_{st.i} - R_{st.i-1}\left[\frac{\varphi_{st.i-1}}{A_{st}}\right] * \varphi_{st.i-1} + (u_{st.i} - u_{st.i-1}) \quad (7)$$

$$0 = R_{pm} * \varphi_{pm.j} - R_{pm} * \varphi_{pm.j-1} + R_{rt.j}\left[\frac{\varphi_{rt.j}}{A_{rt}}\right] * \varphi_{rt.j} - R_{rt.j-1}\left[\frac{\varphi_{rt.j-1}}{A_{rt}}\right] * \varphi_{rt.j-1} + \left(u_{rt.j} - u_{rt.j-1}\right) \quad (8)$$

$$2\mathcal{F}_{pm} = R_{ry.2}\left[\frac{\varphi_{ry.2}}{A_{ry.2}}\right] * \varphi_{ry.2} + R_{rc.1}\left[\frac{\varphi_{rc.1}}{A_{rc.1}}\right] * \varphi_{rc.1} + R_{rc.2}\left[\frac{\varphi_{rc.2}}{A_{rc.2}}\right] * \varphi_{rc.2} + R_{pm} * \varphi_{pm.j+1} + R_{pm} * \varphi_{pm.j+2} + R_{rt.j+1}\left[\frac{\varphi_{rt.j+1}}{A_{rt}}\right] * \varphi_{rt.j+1} + R_{rt.j+3}\left[\frac{\varphi_{rt.j+3}}{A_{rt}}\right] * \varphi_{rt.j+3} + \left(u_{rt.j+1} - u_{rt.j+2}\right) \quad (9)$$

where φ_{ry} , φ_{rc} and $\mathcal{F}_{pm}$ are the rotor yoke flux, the rotor core flux and the magnetic potential of PM poles respectively. Also, R_{st} , R_{sy} , R_{rt} , R_{ry} and R_{rc} are the inherently nonlinear reluctances of the stator teeth and yoke, the rotor teeth, yoke and cores respectively and as seen, these reluctances are dependent on core fluxes.

As mentioned above, by driving the KCL equations of each air gap nodes of the stator and rotor cores, and the KVL equations of each loops of the

stator and rotor cores together, the total algebraic equations are resulted.

2.1.2 The Dynamical Differential Equations of PMSM

The dynamic behaviors of an electrical machine, due to their storage elements, are defined by the differential equations of the mechanical and electrical fields. In fact, the electrical differential equations are the relationship between the induced voltages in the windings and the fluxes passing through those windings, and the mechanical differential equations are the relationship between the variations of rotor displacement angle and the electromagnetic torque. It should be noted that these equations are first order, and most of them are nonlinear. The system of electrical differential equations can be expressed in vector form by:

$$v_s = R_s i_s + \frac{d}{dt}\Lambda_s \tag{10}$$

Here v_s denotes the vector of applied voltages, R_s is the matrix of winding resistances, i_s is the vector of currents in the windings and Λ_s is the vector of flux linkages. If, f, denotes a general symbol, these Introducing vectors is defined as:

$$f_s = [f_a \;\; f_b \;\; f_c]^T \tag{11}$$

The mechanical differential equations for a rotating machine yield:

$$\frac{d\theta}{dt} = \omega \tag{12}$$

$$J\frac{d\omega}{dt} = T_{em} - T_l \tag{13}$$

where θ, ω, J, T_l and T_{em} are the rotor displacement angle, angular speed, total inertia on the shaft, the load torque on the shaft, and the electromagnetic torque, respectively.

Also, the electromagnetic torque of a rotational electrical machine will be generated if any of the air gap flux tube's dimensions is changed and thus, is a function of derivatives of air gap permeances by the rotor displacement angle, θ, as long as there is an mmf drop on each them as following:

$$T_{em} = \sum_{i=1}^{21}\sum_{j=1}^{16}\left(u_i^{st} - u_j^{rt}\right)^2 \frac{dG_{i.j}(\theta)}{d\theta} \tag{14}$$

It is important that, one can see the algebraic equations resulting from the reluctance network and the differential equations of the dynamical behaviors are nonlinear and completely dependent on another one that cannot be solved by the analytical solution methods. Therefore, this system of equations must be solved simultaneously and numerically. In this way, by obtaining all the algebraic and differential equations governing the magnetic, electrical and mechanical equivalent circuit of the machine, a comprehensive analysis of the machine behavior can be resulted. In the following sections, the results of this modeling will be evaluated in several conditions, and also, another numerical method, the finite element analysis method, which will be described in brief, will be used for validation.

2.2 Finite Element Analysis Technique

The finite element analysis method (FEM) is a numerical solution technique for evaluating performance of a wide range of engineering applications. Lately, this method is considered as an important tool to investigate the structures with complex geometry, due to its high capability and flexibility. Although in contrast to the advantages of FEM to compute dynamics of electrical machine, the long computation time necessary is still the main limit to a wider acceptance of this method, which in many applications of optimization and online behavior analysis will be challenge. However, in this paper, the two-dimensional FEM will be used to prove and validate the proposed magnetic equivalent circuit modeling.

In the FEM technique, the electromagnetic structure of the machine is first broken into small finite components, which are called elements, and whatever these elements are selected smaller, cause the higher accuracy and longer time of analysis. Accordingly, the discretizing or the mesh plot of the electromagnetic structure of the studied PMSM machine and its flux density graph are resulted as shown in Fig. 4. Then by applying the Maxwell equations in to all finite elements of electromagnetic structure, the magnetic field behavior and flux distribution in throughout PMSM machine construction can be concluded. In this article, Maxwell Software is used to investigate of different modes of PMSM machine conditions and also, used to evaluate the accuracy of the MEC results.

3 Investigation Proposed MEC Modeling of PMSM Machine

Table 1 shows the dimensional information and parameters of a three-phase, four-pole, PMSM machine. In this section, first, the accuracy of proposed MEC modeling of an interior PMSM machine as modeled in the previous sections, in a healthy and symmetrical conditions is evaluated.

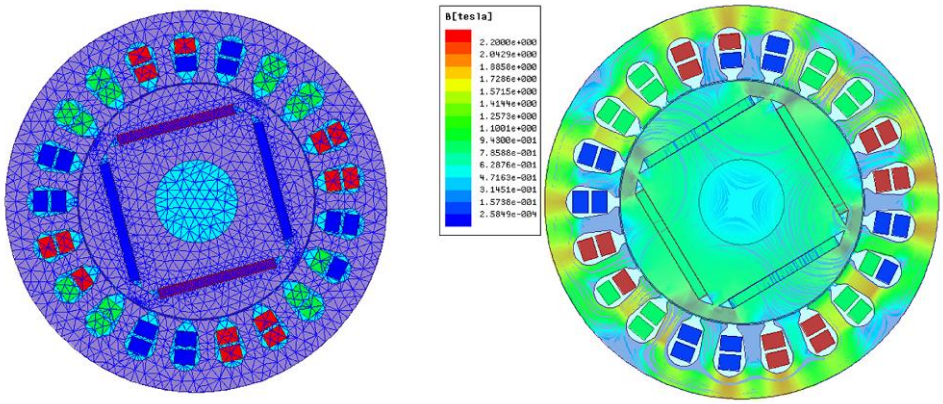

(a) (b)

Fig. 4 a) Plot mesh b) Flux density graph of the studied PMSM.

Table 1 The nominal parameters and dimensional information of PMSM

Quantity	Value
Output power	500 W
Number of pole	4
Slot Numbers	21
Rated speed	1500 rpm
Rated phase current	9 A
Phase number	3
Number of turns of each phase coil	150
Stator outer diameter (D_{so})	120 mm
Stator inner diameter (D_{si})	75 mm
Rotor outer diameter (D_{ro})	74 mm
Rotor inner diameter (D_{ri})	26 mm
Stack length	65 mm
Permanent Magnet	NdFeB
PM length	3 mm
Air gap length	0.5 mm

For this purpose, three-phase currents diagram of the stator windings and the produced electromagnetic torque are resulted according to the full load condition as shown in Figs 5 and 6 respectively. As can be seen in Fig. 6, the electromagnetic torque curve that, resulted from MEC modeling, is also compared with FEM technique, which is well shown the acceptable accuracy of the presented case study MEC model. Also, the spent time in the MEC is much less than the time required for simulation with the finite element software. Due to flexibility of the MEC method in different status, thus, it is possible to evaluate the machine behavior under the influence of different error condition, specially can be analyzed the rotor eccentricity fault and its effect on machine performance. In the next section, the eccentricity fault of rotor is evaluated in different situations.

3.1 Rotor Eccentricity Fault

An eccentricity fault occurs in the electrical machine when a displacement between the cylindrical centers of the stator and rotor is taken place and hence the air gap symmetry is destroyed. In this status, the rotation axis of the rotor is displaced relative to the stator.

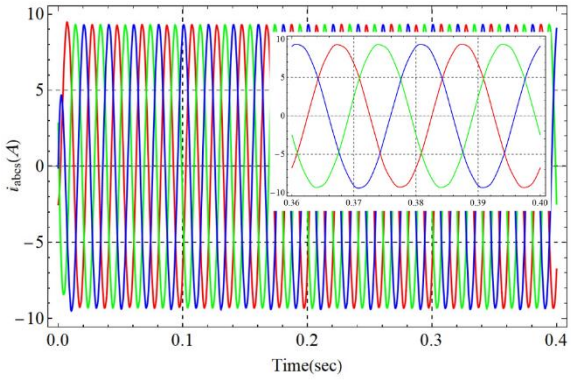

Fig. 5 Full load three-phase current of PMSM in healthy condition.

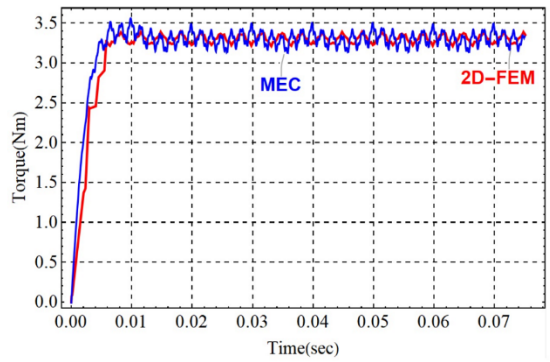

Fig. 6 Produced torque of PMSM in full load and healthy condition.

This displacement causes the unbalanced distribution of the linkage fluxes between the stator and rotor cores, and therefore extends a serious effect on the machine behavior, especially produces the vibration and noise on the output torque. Eccentricity faults mainly have been categorized in various literatures as static eccentricity (SE), dynamic eccentricity (DE) and mixed eccentricity (ME).

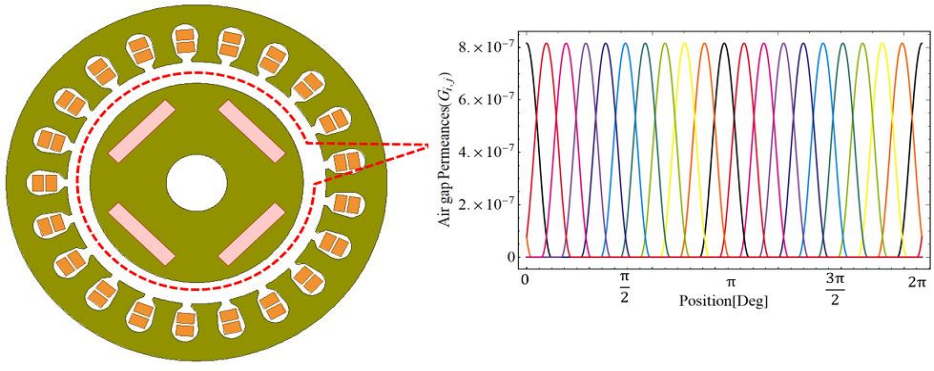

(a) (b)

Fig. 7 a) Symmetrical position of PMSM in healthy condition and b) Permeances between stator and rotor teeth.

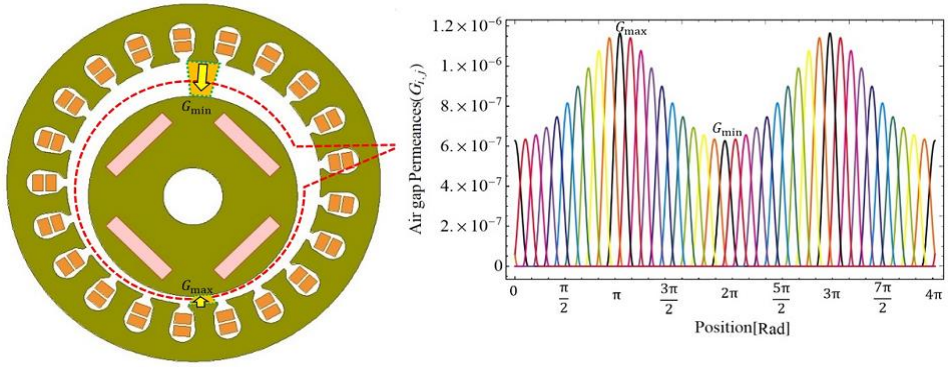

(a) (b)

Fig. 8 a) Unsymmetrical position of PMSM in static eccentricity fault, and b) Permeances between stator and rotor teeth.

In static eccentricity, the displacement between the stator and rotor center has a constant value and for dynamic eccentricity, the minimum distance of the air gap rotates with the rotation of the rotor. Accordingly, when these phenomena are happened together, leads to the mixed eccentricity. In this paper, these types of eccentricity fault are investigated using the magnetic equivalent circuit method for an interior PMSM. The symmetrical position of the rotor and stator centers relative to each other in the healthy condition is shown in Fig. 7-a. As shown in this figure, the air gap is perfectly uniform (the air gap is plotted larger for better representation), and this results in the same values of the magnetic conductions (permeances) between the stator and rotor teeth as illustrated in Fig. 7-b.

3.2 Modeling of Static Eccentricity Fault

The static eccentricity fault of rotor occurs often in installing the electrical machine horizontally and the deficiency of the machine bearings which creating the axial force in the vertical direction. In this case, the rotor core is removed from the center and causes the air gap between the rotor and stator to decrease on one side and increase on the other side. Thus, the rotation axis of the rotor corresponds to its axis of symmetry, but is displaced relative to the stator center as shown in Fig. 8-a. As shown in this figure, the air gap is not constant, and this results in non-uniformly distribution of the magnetic conductions between the stator and rotor teeth as illustrated in Fig. 8-b. The side where the rotor is close to the stator has the highest magnetic conductivity and the side where the rotor is far from the stator, has the least magnetic conductivity. In this way, the static eccentricity fault can be modeled by presenting the appropriate relation of air gap length as follows. According to the diagram in Fig. 8, the proposed relation of air gap length must be time invariant and is depended to rotor position as:

$$L_g(\theta) = L_{g0}(1 + \delta\, cos(\theta)) = L_{g0}(1 + \delta\, cos\, \omega_r t) \quad (15)$$

where L_{g0} is the initial air gap length in healthy condition, θ is the rotor position, ω_r is the angular velocity, and δ is the value of the positive error coefficient in the static eccentricity state. In the healthy condition, the value of δ is equal to zero, and by changing its value from zero to one, the fault percent can be changed from zero to 100%. For example, here the fault of 35% of the rotor deviation from the normal center of under study machine for static eccentricity is evaluated. In this case, using

Equation (15), the length of the air gap between the rotor and stator is expressed as:

$$L_g[\theta] = 0.5\,(1 + 0.35\,Cos[\omega_r t]) \times 10^{-3} \quad (16)$$

The diagram of air gap length in 35% static eccentricity is resulted as Fig. 9.

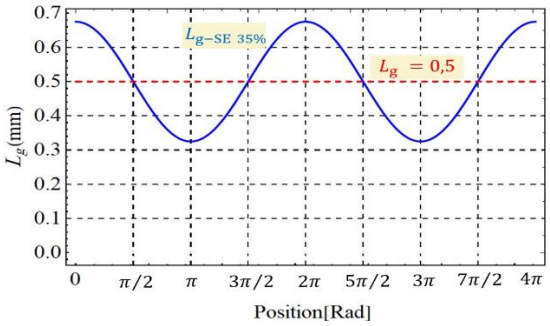

Fig. 9 Diagram of air gap length in 35% static eccentricity.

The faulty PMSM machine performance in 35% static eccentricity case has been evaluated in the MEC modeling, as well as the stator currents and the output torque have been shown in Figs. 10 and 11, respectively. As it can be seen, unsymmetrical stator currents are produced due to the rotor eccentricity fault where an oscillation is mounted on the currents amplitude with a frequency lower than the base frequency value, and therefore, this fault is detectible by stator currents signature analysis. Also, referring Fig. 11, it is very clear that the torque oscillation has been increased and the average torque range has moreover changed from the nominal value.

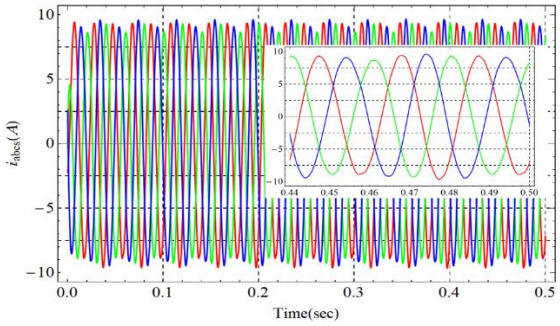

Fig. 10 Stator currents in 35% static eccentricity.

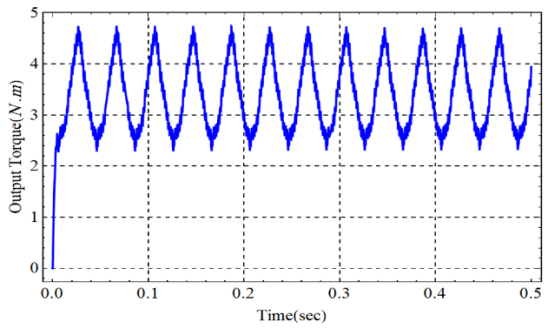

Fig. 11 Output torque in 35% static eccentricity.

If the amount of static eccentricity fault changes from the normal case to maximum of 80% of the healthy state, the magnitude of torque ripples and the torque average amplitude in all modes are simulated and summarized as a function of fault percentage as shown in Fig. 12. As can be seen in this figure, corresponding to increasing the eccentricity fault percentage, the value of output torque average and ripple is increased. This is due to the unbalanced distribution of the linkage fluxes which, creating the vertical forces between the stator and rotor cores.

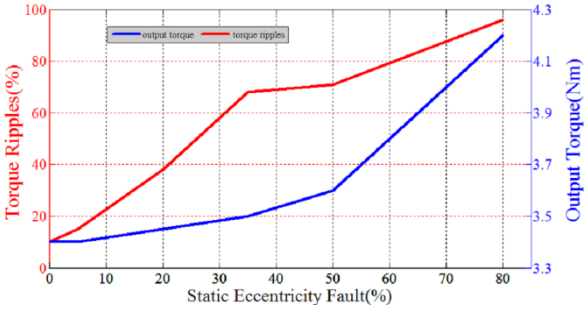

Fig. 12 Effect of static eccentricity fault on output torque average and ripple.

3.3 Modeling of Dynamic Eccentricity Fault

The dynamic eccentricity fault of rotor may be due to improper placement of bearings, the stator and rotor ovalization, and misalignment of the load and rotor shaft which leads to unbalanced magnetic forces in the horizontal and vertical directions. Therefore, the deformed air gap between the rotor and stator can be decreased on one side and increased on the other side as a function of time alternately. In this case, the rotation axis of the rotor is changed constantly, according to the stator center as illustrated in Fig. 13-a. So, the magnetic conduction diagram of an instance permeance between a stator and rotor teeth at three different times is shown in Fig. 13-b. As is clear, in this case, the amplitude of air gap permeances are changed alternatively relative to time, unlike static eccentricity fault. In this way, the dynamic eccentricity fault can be modeled according to the diagram in Fig. 13, which, the relation of air gap length must be time variant and depended to rotor position as:

$$L_{gd}(t) = L_{g0}(1 + a\ cos(b\ w_r t)) \quad (17)$$

where $\boldsymbol{a}$ and $\boldsymbol{b}$ are the positive constant coefficients that, $\boldsymbol{a}$, determines the amount of rotor eccentricity fault and, $\boldsymbol{b}$, determines the frequency of fault variations. In the healthy condition, the value of $\boldsymbol{a}$ is equal to zero, and by changing its value from zero to one, the fault percent can be changed from zero to 100%.

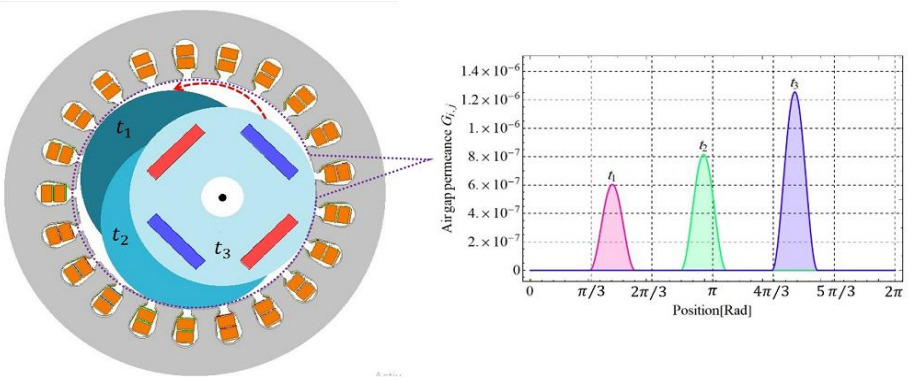

a) b)

Fig. 13 a) Rotor unsymmetrical position of PMSM and b) Permeances between the stator and rotor teeth in dynamic eccentricity fault.

But, the coefficient ***b***, determines the amount of oval movement of rotor from circularity movement or the rate of change of eccentricity fault relative to the base frequency of the machine rotation. If this coefficient is equal to one, the frequency of oval movement of rotor is the same as the synchronous frequency, it means that the point where the rotor is close to the stator and also the point where the rotor is far away from the stator always remains constant and therefore this is a static eccentricity fault as Eq. (15). But when the frequency of oval movement of rotor is other than the synchronous frequency, the point where the rotor approaches the stator or moves away from it, constantly changes and causes different amount of the output torque ripples at different frequencies. As seen, by changing coefficient ***b***, different dynamic eccentricity faults can be achieved. For example, here the fault of 35% of the rotor deviation from the normal center of under study machine with half frequency of fault variations is evaluated as:

$$L_{gd}(t) = 0.5 \times (1 + 0.35\, Cos(0.5\, w_r t)) \quad (18)$$

The faulty PMSM machine performance in 35% dynamic eccentricity case has been evaluated in the MEC modeling, as well as the stator currents and the output torque have been shown in Figs. 14 and 15, respectively.

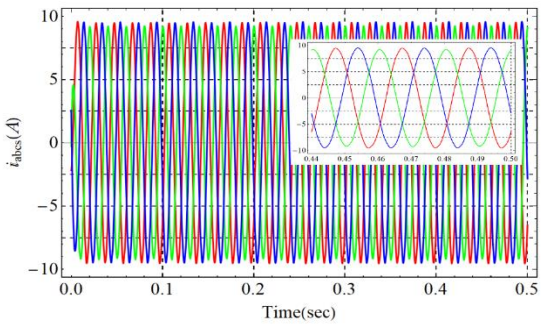

Fig. 14 Stator currents in 35% dynamic eccentricity.

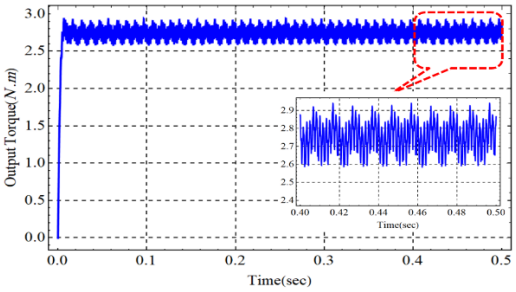

Fig. 15 Output torque in 35% dynamic eccentricity.

Referring these figures, it is very clear that the average torque amplitude has increased and the torque ripple has been decreased unlike the corresponding static eccentricity fault.

If the amount of dynamic eccentricity fault changes from the normal case to maximum of 80% of the healthy state, the magnitude of torque ripples and the torque average amplitude are simulated and summarized as a function of fault percentage as shown in Fig. 16. As can be seen in this figure, corresponding to increasing the eccentricity fault percentage, the value of output torque average is decreased and the value of output torque ripple is increased. This is due to the disturbance in the air-gap field distribution which, causes the unbalanced radial forces between the stator and rotor and, thus, some signals within the motor.

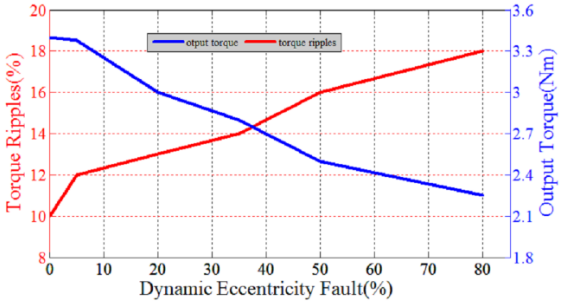

Fig. 16 Effect of dynamic eccentricity fault on output torque average and ripple.

3.4 The Effect of Dynamic Eccentricity Frequency on Torque Ripple

In order to observe the effect of different level of dynamic eccentricity fault on output torque ripple, the introduced MEC model is applied in the dynamic eccentricity condition at different frequencies. The coefficient ***b***, in the proposed Eq. (17), determines the rate of change of eccentricity fault relative to the base frequency of the machine rotation. In fact, this coefficient is varied in different conditions of eccentricity fault and depends on the condition of the faulty electric machine. Since, in this section, the coefficient ***b***, is gradually increased from the value of 0 to 5, where, the frequencies amplitude are varied from zero to five times the main frequency, namely, 250 Hz. Fig. 17 shows the variation of the amplitudes of the output torque ripples in different level (or different frequency) of dynamic eccentricity fault at full load and 35% DE.

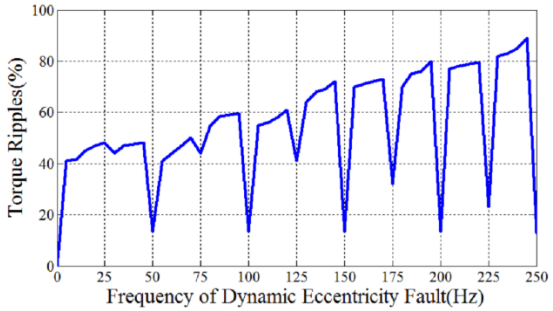

Fig. 17 Variation of the output torque ripples in different level of dynamic eccentricity.

Consequently, referring to Fig. 17, it is clear that, the appearing fault and the frequency of variation, indicates the fault degree. As can be seen in this figure, if the coefficient ***b***, or the frequency of fault variations is a positive integer multiple of the main frequency, the torque ripple value is decreased. But if the coefficient ***b***, or the frequency of fault variations is a positive non-integer, the torque ripple value is increased. By investigating of results it seems that in the integer multiple of the main frequency, the dynamic eccentricity faults have turned into a static eccentricity faults, which it remains almost constant at a certain value. According to this resultant, it was pondered that the frequency of eccentricity faults can affect the output torque ripples.

4 Conclusion

In this paper, the detailed modeling of an interior PMSM using the MEC was introduced. The merit of the proposed MEC model is considering the core saturation and the distribution of air gap permeances that, leading to more detailed calculated torque. The time-domain results in MEC as well as FEM were compared and it was shown that the results of the presented MEC model is closer to that of the FEM. This indicates the efficiency of the proposed MEC method as it has a higher speed and acceptable accuracy. Finally, several cases of eccentricity fault in a PMSM motor was illustrated. According to the simulation results, it was observed that the rotor eccentricity faults can affect the output torque and stator current of the machine. So, the eccentricity fault detection is simple by solely analyzing the output torque and the stator current compared with the healthy status.

Intellectual Property

The authors confirm that they have given due consideration to the protection of intellectual property associated with this work and that there are no impediments to publication, including the timing to publication, with respect to intellectual property.

Funding

No funding was received for this work.

CRediT Authorship Contribution Statement

V. Naeini: Idea & Conceptualization, Data Curation, Analysis, Project Administration, Software and Simulation, Supervision, Verification, Original Draft Preparation, Revise & Editing. **M. Momeni:** Research & Investigation, Data Curation, Analysis, Simulation, Verification, Original Draft Preparation.

Declaration of Competing Interest

The authors hereby confirm that the submitted manuscript is an original work and has not been published so far, is not under consideration for publication by any other journal and will not be submitted to any other journal until the decision will be made by this journal. All authors have approved the manuscript and agree with its submission to “Iranian Journal of Electrical and Electronic Engineering”.

References

[1] B. N. Cassimere, S. D. Sudhoff and D. H. Sudhoff, "Analytical Design Model for Surface-Mounted Permanent-Magnet Synchronous Machines", *IEEE Transactions on Energy Conversion*, Vol. 24, No. 2, pp. 347-357, 2009.

[2] A. Daghigh, H. Javadi and A. Javadi, "Improved Analytical Modeling of Permanent Magnet Leakage Flux in Design of the Coreless Axial Flux Permanent Magnet Generator," *Canadian Journal of Electrical and Computer Engineering*, Vol. 40, No. 1, pp. 3-11, 2017.

[3] V. Naeini, Y. S. Ayat , "Computation of the EMF in an Axial Flux PM less Machine using Analytical Method", *Tabriz Journal of Electrical Engineering*, Vol. 50, No. 2, pp. 935-941, 2020.

[4] A. Jabbari "The Effect of Dummy Slots on Machine Performance in Brushless Permanent Magnet Machines: An Analytical, Numerical, and Experimental Study". *Iranian Journal of Electrical and electronic Engineering*, Vol. 18, No. 2, pp. 1–11, 2022.

[5] A. Jabbari and F. Dubas, "New Subdomain Method for Performances Computation in Interior Permanent-Magnet (IPM) Machines", *Iranian Journal of Electrical and electronic Engineering*, Vol. 16, No. 1, pp. 26–38, 2020.

[6] W. Tong, S. Wang, S. Dai, S. Wu and R. Tang, "A Quasi 3-D Magnetic Equivalent Circuit Model of a Double-Sided Axial Flux Permanent Magnet Machine Considering Local Saturation," *IEEE Transactions on Energy Conversion*, Vol. 33, No. 4, pp. 2163-2173, 2018.

[7] V. Ostovic, Dynamics of saturated electric machines. New York, N.Y.: Springer, 1989.

[8] J. Bao, B. L. J. Gysen and E. A. Lomonova, "Hybrid Analytical Modeling of Saturated Linear and Rotary Electrical Machines: Integration of Fourier Modeling and Magnetic Equivalent Circuits," *IEEE Transactions on Magnetics*, Vol. 54, No. 11, pp. 1-5, 2018.

[9] J. Nazarzadeh and V. Naeini, "Magnetic Reluctance Method for Dynamical Modeling of Squirrel Cage Induction Machines" M.Chomat,ed., InTech,Croatia, pp. 41-60, 2011.

[10] V. Naein, "A detailed magnetic equivalent circuit modeling for torque ripples minimizing of a switched reluctance motor", *International Transaction on electrical energy system*, Vol. 30, No. 1, pp.1-14, 2020.

[11] F. R. Alam, B. Rezaeealam, S. M. M. Moosavi, "An Improved Magnetic Equivalent Circuit Model for Electromagnetic Modeling of Electric Machines", *Iranian Journal of Electrical and Electronic Engineering*, Vol. 17, No. 3, pp. 1-14, 2021.

[12] F. R. Alam, and B. Rezaeealam, "An enhanced analytical technique based on winding function theory for analysis of induction motors". *International Transactions on Electrical Energy Systems*, Vol. 31, 2021.

[13] J. Faiz, and F. R. Alam, "A new hybrid analytical model based on winding function theory for analysis of surface mounted permanent magnet motors", *International Journal of Computational Materials Science and Engineering (COMPEL)*, Vol. 38, No. 2, pp. 745-758, 2019.

[14] K. Abbaszadeh, and F. R. Alam, "On-load field component separation in surface-mounted permanent-magnet motors using an improved conformal mapping method", *IEEE Transactions on Magnetics*, Vol. 52, No. 2, 2016.

[15] R. Wang, S. Pekarek, P. O'Regan, A. Larson and R. van Maaren, "Incorporating Skew in a Magnetic Equivalent Circuit Model of Synchronous Machines," *IEEE Transactions on Energy Conversion*, Vol. 30, No. 2, pp. 816-818, 2015.

[16] Y. Huang, T. Zhou, J. Dong, H. Lin, H. Yang and M. Cheng, "Magnetic Equivalent Circuit Modeling of Yokeless Axial Flux Permanent Magnet Machine With Segmented Armature," *IEEE Transactions on Magnetics*, Vol. 50, No. 11, pp. 1-4, 2014.

[17] H. Saneie, Z. N. Gheidari and F. Tootoonchian, "Design-Oriented Modelling of Axial-Flux Variable-Reluctance Resolver Based on Magnetic Equivalent Circuits and Schwarz–Christoffel Mapping," *IEEE Transactions on Industrial Electronics*, Vol. 65, No. 5, pp. 4322-4330, 2018.

[18] F. A. Kharanaq, R. A. Sarabi, Z. N. Gheidari and F. Tootoonchian, "Magnetic Equivalent Circuit Model for Wound Rotor Resolver Without Rotary Transformer's Core," *IEEE Sensors Journal*, Vol. 18, No. 21, pp. 8693-8700, 2018.

[19] Zhongming, Y.; Bin, W. "A Review on Induction Motor Online Fault Diagnosis", *In Proceedings of the IPEMC Third International Power Electronics and Motion Control Conference (IEEE Cat. No.00EX435)*, Beijing, China, pp. 1353–1358, August 2000.

[20] B. M. Ebrahimi, J. Faiz, and M. J. Roshtkhari, "Static-, Dynamic-, and Mixed-Eccentricity Fault Diagnoses in Permanent-Magnet Synchronous Motors," *IEEE Transactions on Industrial Electronics*, Vol. 56, No. 11, pp. 4727-4739, 2009.

[21] B. M. Ebrahimi, M. J. Roshtkhari, J. Faiz, "Advanced eccentricity fault recognition in permanent magnet synchronous motors using stator current signature analysis", *IEEE Transactions on*

Industrial Electronics., Vol. 61, No. 4, pp. 2041-2052, 2014.

[22] H. Mahmoud and N. Bianchi, "Eccentricity in synchronous reluctance motors—Part I: analytical and finite-element models", *IEEE Transactions on Energy Conversion*, Vol. 30, No. 2, pp. 745-753, 2015.

[23] F. Tootoonchian, F. Zare, "Performance Analysis of Disk Type Variable Reluctance Resolver under Mechanical and Electrical Faults", *Iranian Journal of Electrical and electronic Engineering*, Vol. 14, No. 3, pp. 299-307, 2018.

[24] M. Ojaghi and S. Nasiri, "Modeling eccentric squirrel-cage induction motors with slotting effect and saturable teeth reluctances", *IEEE Transactions on Energy Conversion*, Vol. 29, No. 3, pp. 619-627, 2014.

[25] J. Faiz , B. M. Ebrahimi , and H. A. Toliyat, "Effect of magnetic saturation on static and mixed eccentricity fault diagnosis in induction motor", *IEEE Transactions on Magnetics*, Vol. 45, No. 8, pp. 3137-3144, 2009.

[26] E. Ajily, M. Ardebili, and K. Abbaszadeh, "Magnet defect and rotor eccentricity modeling in axial flux permanent magnet machines via 3D field reconstruction method", *IEEE Transactions on Energy Conversion*, Vol. 31, No. 2, pp. 486-495, 2016.

[27] A. Rahideh and T. Korakianitis, "Analytical open-circuit magnetic field distribution of slotless brushless permanent-magnet machines with rotor eccentricity", *IEEE Transactions on Magnetics*, Vol. 47, No. 12, pp. 4791-4808, 2011.

V. Naeini was born in Hamedan, Iran, in 1984. He received the B.Sc. and M.Sc. degrees in electrical engineering from Shahed University, Tehran, Iran, in 2006 and 2009, respectively. He received the Ph.D. degree in electrical engineering from K. N. Tosi University of Technology, Tehran, Iran, in 2016. Since 2016, he has been an Assistant Professor with the Electrical Engineering at Malayer University, Hamedan, Iran. His main research interests include design, modeling and analysis of electrical machines and power transformers.

M. Moomeni was born in Malayer, Hamedan, Iran, in 1989. He received the B.Sc. and M.Sc. degrees in electrical engineering from Malayer University, Hamedan, Malayer, Iran, in 2017 and 2019, respectively. His main research interests include design, modeling and analysis of electrical machines and power transformers.